1.1 Characterization

X-ray diffraction (XRD) patterns were collected on Aeris (PANalytical) with Cu Kα radiation (λ = 0.154 nm). Raman spectra were collected on LabRAM HR Evolution (Horiba) with a 532-nm laser device. The zeta potential was collected by Zetasizer Nano (Malvern). X-ray photoelectron spectra (XPS) was acquired on Escalab 250Xi (Thermo Fisher) with a pass energy of 40.0 eV and an energy step of 0.05 eV. The scanning electron microscope (SEM) images were conducted by SU8220 (Hitachi) under 15 kV. The transmission electronic microscopy (TEM) images were captured by Talos F200S (FEI Thermo) under an acceleration voltage of 200 kV.

1.2 Electrochemical measurements

After mixing 4 mg of the sample with 200 μl of ultrapure water, 750 μl of ethyl alcohol, and 50 μl of Nafion, the electrode slurry was sonicated for 30 minutes. The slurry was then coated onto a 1 cm^2 carbon paper, with an approximate loading of 2 mg cm^{-2} of active material. The solvent was then dried at 60°C to prepare the working electrode. Electrochemical tests were conducted using a CHI 760E electrochemical workstation (Shanghai Chenhua Instrument Co., Ltd., China) in a 1 M Na_2SO_4 aqueous electrolyte solution, with Ag/AgCl and a carbon rod serving as the reference and counter electrodes, respectively, in a three-electrode system with the sample as the working electrode. Perform cyclic voltammetry (CV) and galvanostatic charge-discharge (GCD) measurements within a potential window of 0.0 to 1.0 V. Utilize the Zahner electrochemical workstation (Germany) for electrochemical impedance spectroscopy (EIS) measurements in the frequency range of 10^{-2}-10^5 Hz. The specific mass capacitance (F g^{-1}) is determined from CV and GCD curves through (Eq. S1) and (Eq. S2) respectively.

$$C = \frac{\int I \times dV}{vm\Delta V} \quad \text{（Eq. S1）}$$

where $\int I \times dV$ is the area under the curve, v is the scanning rate, m is the mass of the active material on the electrode, and ΔV is the potential range.

$$C = \frac{I\Delta t}{m\Delta V} \quad \text{（Eq. S2）}$$

where I is the current density, Δt is the discharge time, m is the mass of the active electrode material, and ΔV is the potential range.

A symmetric supercapacitor was fabricated by assembling K-AMO as the working electrode. Two electrodes were separated by glassy fibrous separator in 1 M Na_2SO_4 aqueous electrolyte. Symmetric supercapacitors were analyzed through cyclic voltammetry (CV) and galvanostatic charge/discharge (GCD) measurements within a potential range of 0.0 to 2.0 V,

utilizing a dual-electrode system on a CHI 760E electrochemical workstation. Button supercapacitor was fabricated by assembling K-AMO as both the anode and cathode. The current collector diameter was 1.2 cm, with an active material loading of 2 mg cm^{-2}, and a separator diameter of 1.6 cm. A small amount of electrolyte was added to complete the assembly of the button supercapacitor. The energy density (Wh kg^{-1}) and power density (W kg^{-1}) of the symmetrical supercapacitor are calculated using equations (Eq. S3) and (Eq. S4):

$$E = \frac{C\Delta V^2}{7.2} \quad \text{（Eq. S3）}$$

$$P = \frac{3600E}{t} \quad \text{（Eq. S4）}$$

where C is the specific capacitance of the symmetrical supercapacitor, ΔV is the measurement potential window, and t is the discharge time.

1.3 The in situ ATR-SEIRAS measurements

In situ ATR-SEIRAS testing is performed on a Nicolet iS50 Fourier transform infrared spectrometer. Using a pillar-shaped prism made of silicon crystal as the main ATR component, a layer of gold film is chemically deposited on the surface of the silicon block (Au@Si) as the working electrode for SEIRAS. The electrochemical system consists of a 1 M Na_2SO_4 aqueous solution, an Ag/AgCl reference electrode, and a carbon rod electrode. In situ ATR-SEIRAS measurements were conducted at room temperature, with the results expressed in absorbance units as A = log (1/T) = -log (R_s/R_0), where R_s and R_0 represent the reflected radiation intensity at the selected electrode potential and the open circuit potential (OCP) spectrum, respectively. The CHI 760E electrochemistry workstation (Shanghai Chenhua Co., Ltd., China) was used for potential control.

1.4 Calculation of capacitance contributions

The relationships between the scan rate and current density were used to investigate the reaction kinetics based on Eq. S5:

$$i = av^b \quad \text{(Eq. S5)}$$

where a and b are constants related to the different electrochemical processes, in which b = 0.5 represents diffusion control while b = 1 belongs to surface control.

To quantify the capacitive contribution to the current response, we could divide the above formula into Eq. S6:

$$i(V) = k_1 v + k_2 v^{1/2} \quad \text{(Eq. S6)}$$

Where i (V) is the current at a certain potential of V, v is the scan rate. k_1 and k_2 correspond

to the capacitive-controlled and diffusion-controlled processes, respectively.

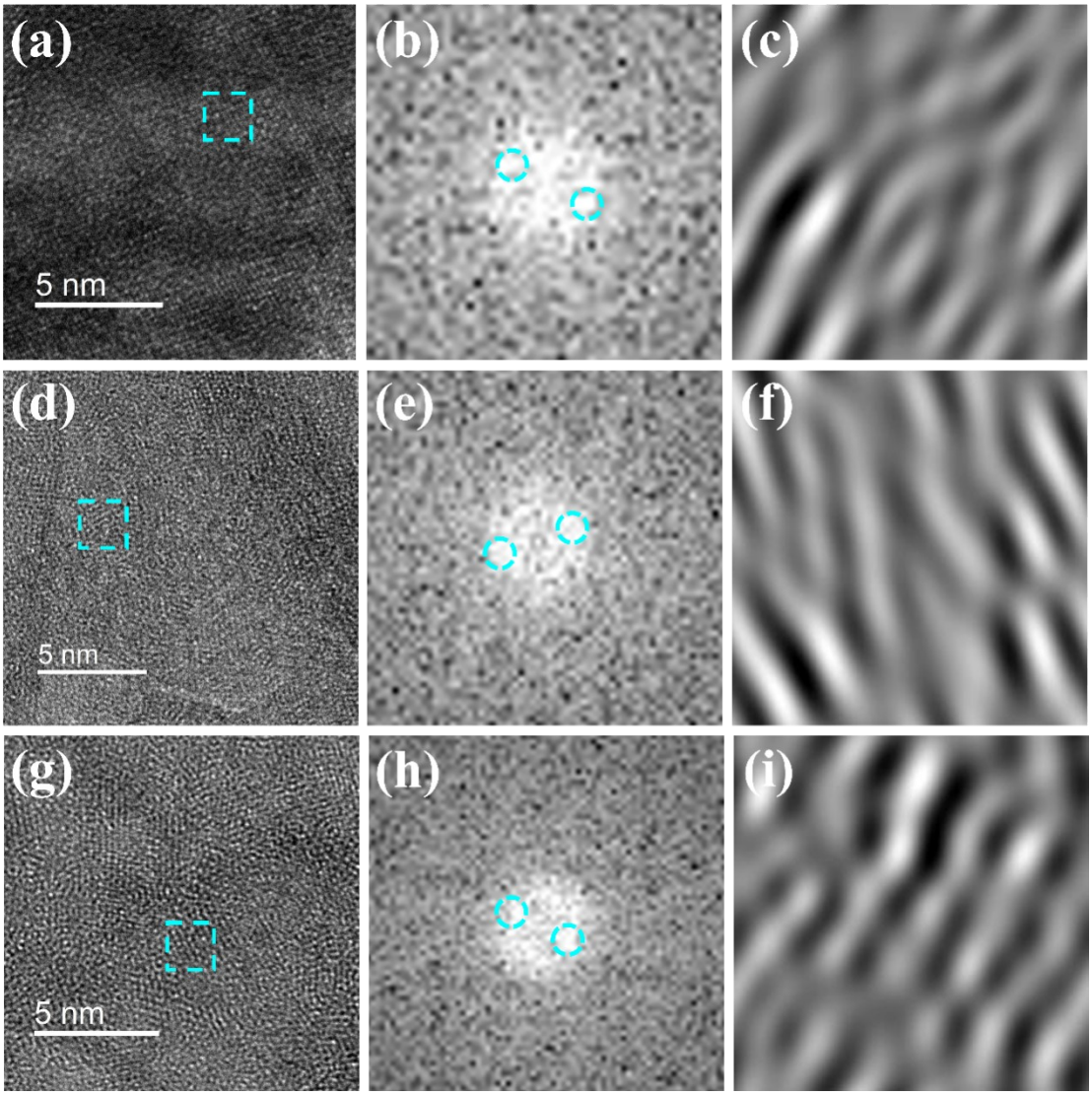

Fig. S1 TEM and Fourier transform images of Na-AMO-OH (a-c), K-AMO-OH (d-f) and Na-AMO (g-i).

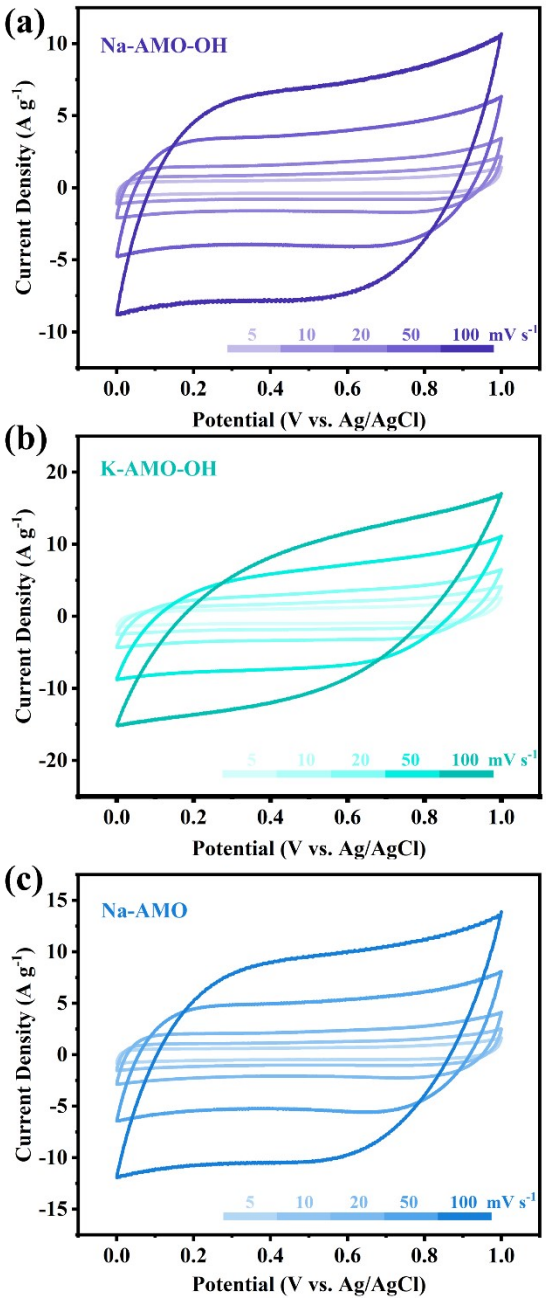

Fig. S2 CV curves of Na-AMO-OH (a), K-AMO-OH (b), and Na-AMO (c) at various scan rates.

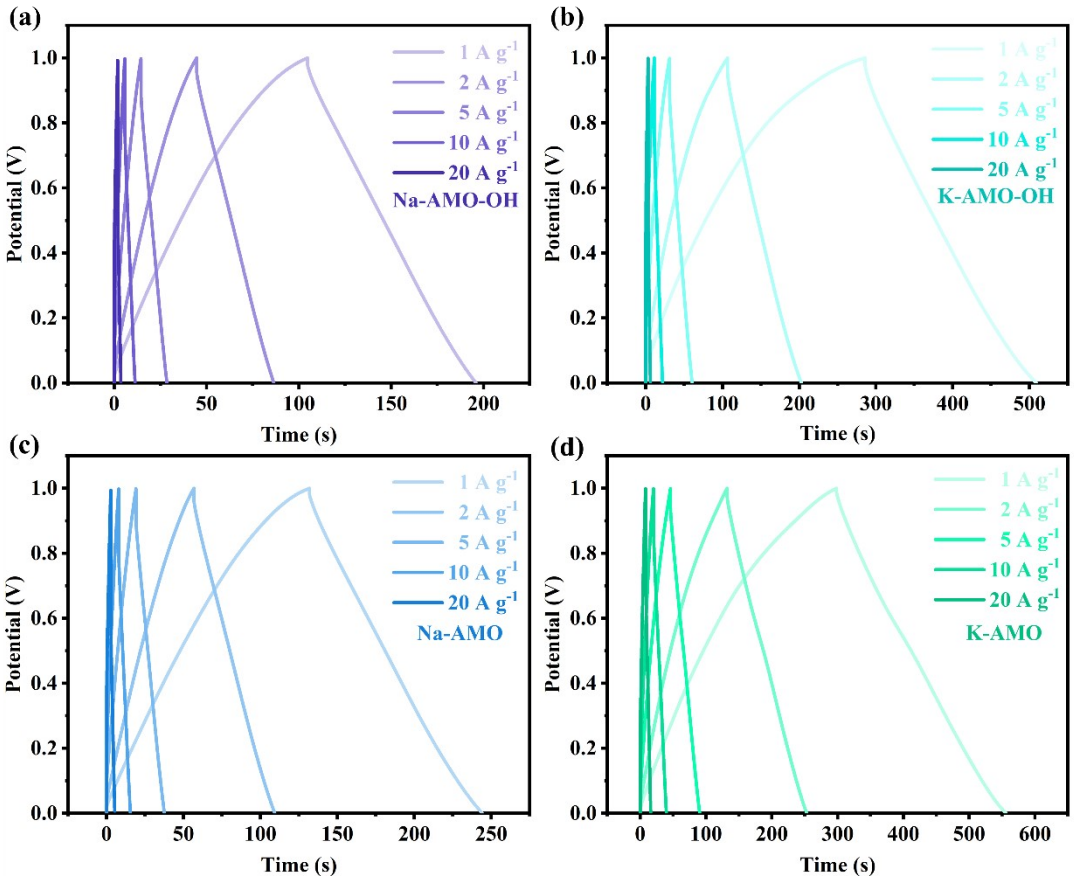

Fig. S3 GCD curves of Na-AMO-OH (a), K-AMO-OH (b), Na-AMO (c), and K-AMO (d) at various current densities.

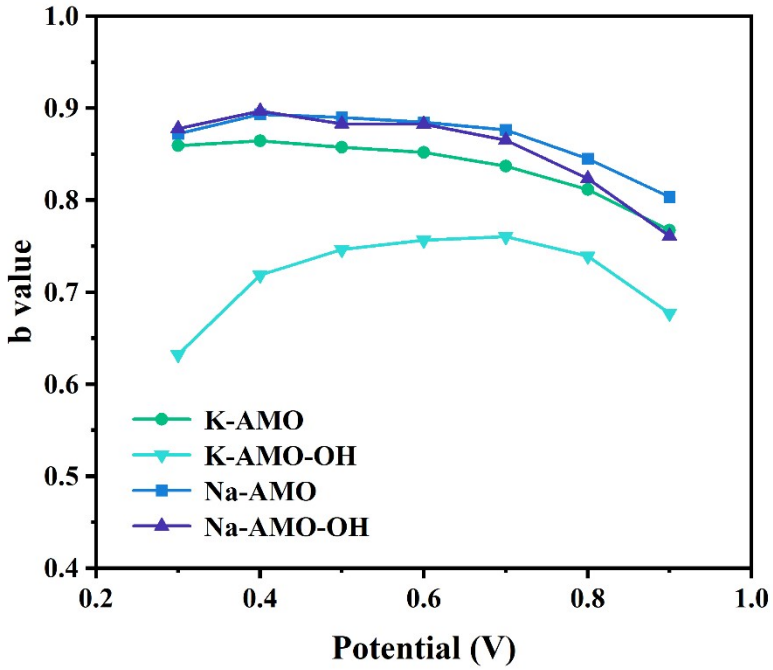

Fig. S4 The b values of four samples at different voltages.

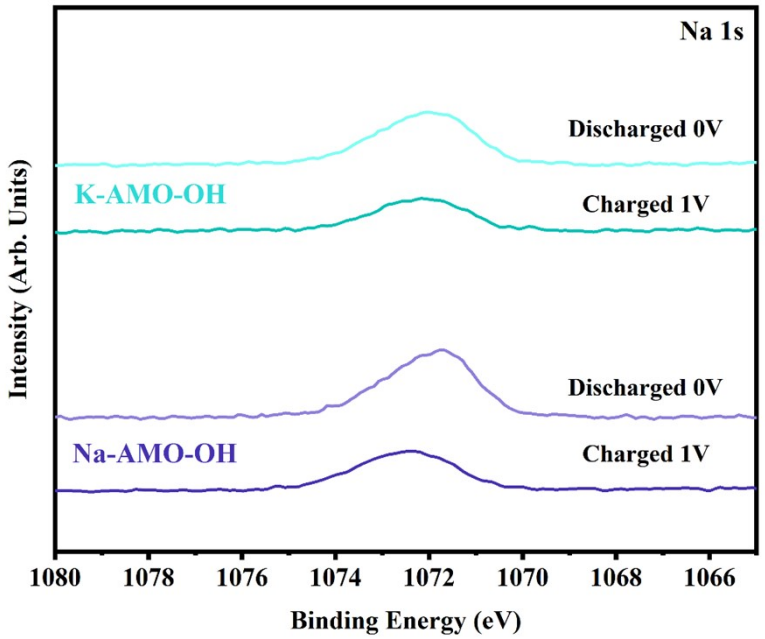

Fig. S5 XPS spectra of Na 1s for K-AMO-OH and Na-AMO-OH samples after charging and discharging.

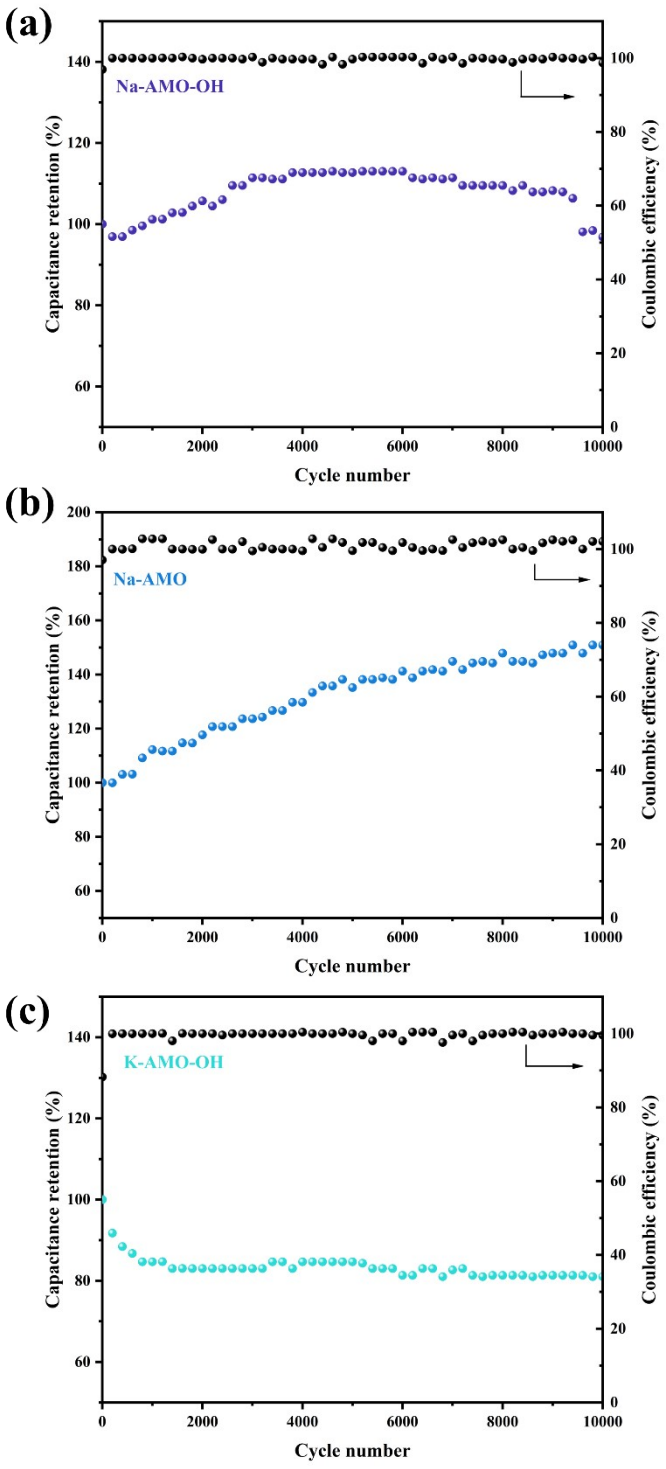

Fig. S6 Cyclic testing graphs of Na-AMO-OH (a), Na-AMO (b), and K-AMO-OH (c) at a current density of 20 A g^{-1} for 10 000 charge-discharge cycles.

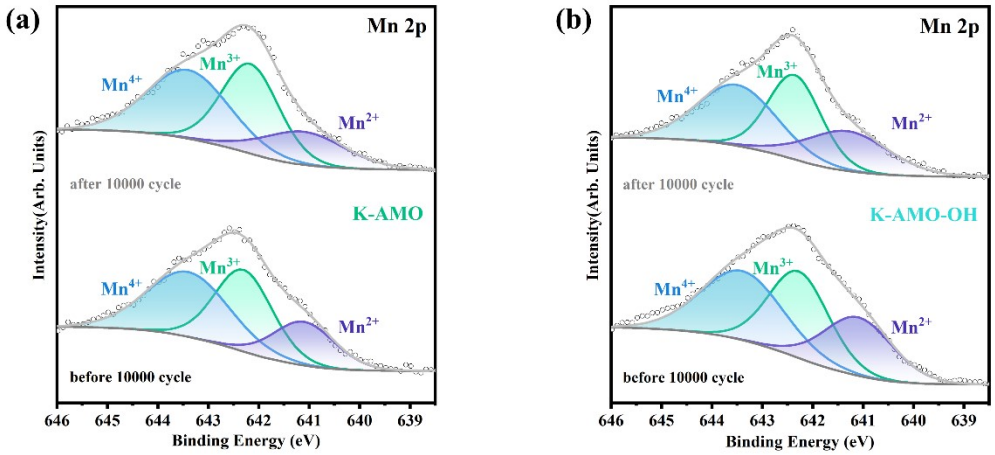

Fig. S7 XPS spectra of Mn 2p for K-AMO (a) and K-AMO-OH (b) after 10 000 cycles of galvanostatic charge-discharge.

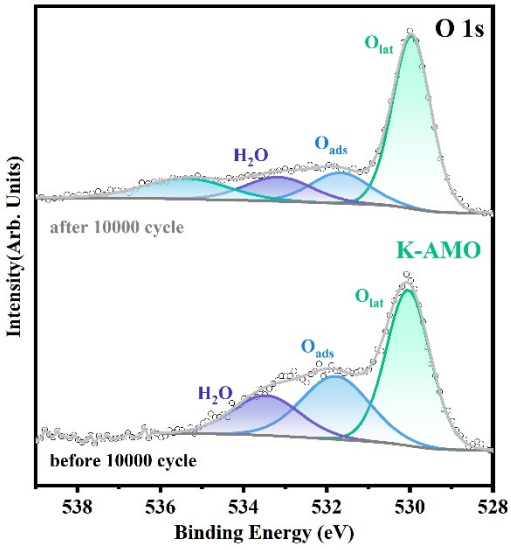

Fig. S8 XPS spectra of O 1s for K-AMO after 10 000 cycles of galvanostatic charge-discharge.

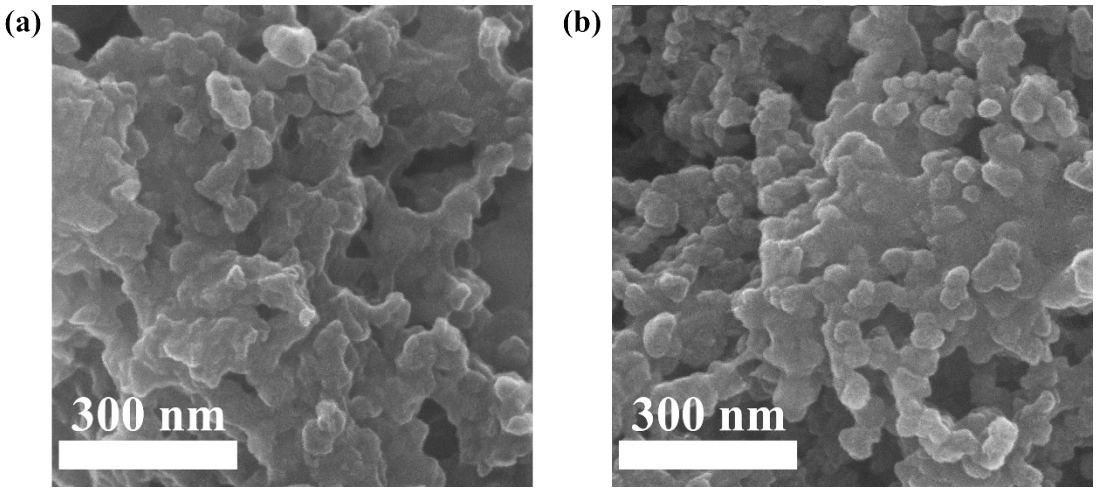

Fig. S9 SEM images for K-AMO (a) and K-AMO-OH (b) after 10 000 cycles of galvanostatic charge-discharge.

Table S1 The specific capacitance calculated by CV at various scan rates.

Scan rate	Specific capacitance (F g^{-1})			
(mV s^{-1})	K-AMO	Na-AMO	K-AMO-OH	Na-AMO-OH
5	258.88	123.08	214.63	99.09
10	242.70	117.03	186.98	91.60
20	225.69	111.40	161.20	84.69
50	195.78	100.18	126.71	74.81
100	164.90	88.13	98.90	66.46

Table S2 The specific capacitance calculated by GCD at various current density.

Current density	Specific capacitance (F g^{-1})			
(A g^{-1})	K-AMO	Na-AMO	K-AMO-OH	Na-AMO-OH
1	258.32	112.57	223.84	91.40
2	242.17	105.13	192.41	83.65
5	221.88	92.59	148.02	70.42
10	196.84	76.69	107.63	55.65
20	158.50	52.68	59.21	35.37

Table S3 Calculation of Coulombic efficiency in GCD tests at various current densities.

Current density ($A\ g^{-1}$)	Columbic efficiencies (%)			
	K-AMO	**Na-AMO**	**K-AMO-OH**	**Na-AMO-OH**
1	87	86	78	87
2	92	93	90	94
5	96	97	95	97
10	98	98	96	98
20	99	98	95	97

Table S4 The calculation results of SSC measured by CV and GCD tests

Scan rate ($mV\ s^{-1}$)	SSC Specific capacitance ($F\ g^{-1}$)	Current density ($A\ g^{-1}$)	SSC Specific capacitance ($F\ g^{-1}$)
5	101.70	1	101.00
10	92.65	2	76.87
20	85.67	5	58.67
50	72.22	10	46.06
100	61.51	20	31.22

Table S5 Electrochemical parameters of SSC.

Current density ($A\ g^{-1}$)	Discharge time (s)	Discharge capacitance ($F\ g^{-1}$)	Energy density ($Wh\ kg^{-1}$)	Power density ($W\ kg^{-1}$)
1	202.00	101.00	56.11	1000.0
2	76.85	76.87	42.70	2000.6
5	23.45	58.67	32.60	5004.2
10	9.2	46.06	25.59	10012.9
20	3.1	31.22	17.34	20143.6

Table S6 EIS test Nyquist diagram fitting results.

Sample	R_s	CPE		R_{ct}	W_o		
		CPE-T	CPE-P		W-R	W-T	W-P
K-AMO	3.24	1.6×10^{-2}	0.65	0.18	2.84	0.39	0.47
Na-AMO	3.40	9.4×10^{-3}	0.69	0.20	1.64	0.20	0.49
K-AMO-OH	3.31	2.3×10^{-2}	0.73	-	1.87	0.26	0.48
Na-AMO-OH	3.48	8.2×10^{-4}	0.97	0.21	2.20	0.38	0.47

Table S7 The comparison between the specific volume in our work and the report.

Material	Method	Specific capacitance	Substrate and electrolyte	Capacitance retention	Mass loading	Ref.
Amorphous MnO_2 nanospheres	Chemical precipitation	252.2 F g^{-1} at 1 A g^{-1}	Ni Foam (1 M Na_2SO_4)	95.1% after 5200 cycles at 5 A g^{-1}	2 mg cm^{-2}	1
Na_xMnO_2	Electrochemical deposition	230 F g^{-1} at 1 A g^{-1}	stainless steel (1 M Na_2SO_4)	64% after 4 cycles at 32 A g^{-1}	-	2
MnO_2	Chemical precipitation	138 F g^{-1} at 1 A g^{-1}	Carbon cloth (1 M Na_2SO_4)	82.8% after 10 000 cycles at 1 A g^{-1}	2 mg cm^{-2}	3
MnO_2-CNT	Chemical precipitation	151.9 F g^{-1} at 5 mV s^{-1}	Ni Foam (1 M Na_2SO_4)	92.8% after 5000 cycles at 2 A g^{-1}	1 mg cm^{-2}	4
MnO_2 NSs@MnO_2 HNPAs	Electrochemical deposition	244.5 F g^{-1} at 0.5 A g^{-1}	Carbon cloth (1 M Na_2SO_4)	120% after 5000 cycles at 1.5 A g^{-1}	1.3 mg cm^{-2}	5
α-Fe_2O_3/MnO_2	Hydrothermal method	216 F g^{-1} at 0.5 A g^{-1}	nickel foil sheet (1 M KOH)	85.1% after 10 000 cycles at 1 A g^{-1}	-	6
CNF/MnO_2	DC reactive sputtering	151.1 F g^{-1} at 1 A g^{-1}	Ni Foam (1 M Na_2SO_4)	93.5% after 1500 cycles at 1 A g^{-1}	-	7
MnO_2@CNT@CF	Electrochemical deposition	213 F g^{-1} at 0.1 A g^{-1}	Carbon fabric (0.5 M Na_2SO_4)	88% after 7000 cycles at 0.5 A g^{-1}	3.37 mg cm^{-2}	8
MnO_2@MXene@CC	Selective etching	234.8 F g^{-1} at 1 A g^{-1}	Carbon cloth (0.5 M Na_2SO_4)	80% after 10 000 cycles at 10 A g^{-1}	0.2 mg cm^{-2}	9
MnO_x/CC	In-situ electrochemical	205.1 F g^{-1} at 1 mA cm^{-2}	Carbon cloth (0.5 M Na_2SO_4)	91.2% after 5000 cycles at 10 mA cm^{-2}	-	10
K-AMO	Chemical precipitation	258.3 F g^{-1} at 1 A g^{-1}	Carbon fiber paper (1 M Na_2SO_4)	104% after 10 000 cycles at 20A g^{-1}	2 mg cm^{-2}	This work

References

1. Q. Ma, M. Yang, X. Xia, H. Chen, L. Yang and H. Liu, *Electrochim. Acta*, 2018, 291, 9-17.
2. M. A. Desai, A. Kulkarni, G. Gund and S. D. Sartale, *Energy Fuels*, 2021, **35**, 4577-4586.
3. A. Zhang, R. Zhao, L. Hu, R. Yang, S. Yao, S. Wang, Z. Yang and Y. M. Yan, *Adv. Energy Mater.*, 2021, **11**.
4. H. Huang, W. Zhang, Y. Fu and X. Wang, *Electrochim. Acta*, 2015, **152**, 480-488.
5. G. Nagaraju, Y. H. Ko, S. M. Cha, S. H. Im and J. S. Yu, *Nano Res.*, 2016, **9**, 1507-1522.
6. M. Racik K, A. Manikandan, M. Mahendiran, J. Madhavan, M. Victor Antony Raj, M. G. Mohamed and T. Maiyalagan, *Ceram. Int.*, 2020, **46**, 6222-6233.
7. P. Ning, X. Duan, X. Ju, X. Lin, X. Tong, X. Pan, T. Wang and Q. Li, *Electrochim. Acta*, 2016, **210**, 754-761.
8. M. Nepal, G. S. Gudavalli and T. P. Dhakal, *ACS Omega*, 2025, **10**, 3439-3448.
9. M. Huang, J. He, Y. Yang, X. Zhang, C. Liang, Y. Lv, D. He and Y. Wang, *J. Phys. Chem. Solids*, 2026, **208**.
10. X. Wu, T. Zhan, S. Sun, W. Chen, A. Yu, S. Qiu, L. Chen, D. Qu, J. Duan and X. Li, *Electrochim. Acta*, 2025, **516**.